Electronic Supplementary Material (ESI) for Soft Matter.
This journal is © The Royal Society of Chemistry 2022

Supporting Information: Long-range Transport and Directed Assembly of Charged Colloids under Aperiodic Electrodiffusiophoresis

Kun Wang,[†] Samuel Leville,[†] Behrouz Behdani,[†] and Carlos A. Silvera Batista[*,†,‡]

†*Department of Chemical and Biomolecular Engineering, Vanderbilt University, Nashville, TN*

‡*Vanderbilt Institute for Nanoscale Science and Engineering*

E-mail: silvera.batista@vanderbilt.edu

Phone: (615) 875-6195

The plots and data shown below complements the following data in the main text: Figures S1-S4 provides the heat maps for pH and intensity profiles for the experiments reported in Fig. 3 and Fig. 5 of the main text. Figures S5-S7 provides the heat maps for pH and intensity profiles that support the discussion in Section 3.3 of the main text. These figures demonstrate that highly nonlinear—and divergent—pH profiles are essential to observe focusing of particles. When solutions are made highly acidic or basic, or when the solution is buffered, changes in pH are minimal. We did not observed focusing in any of those cases. Figure S8 shows the effect of adding indifferent background electrolytes. The rate of accumulation of particles decreases with the addition of NaSCN, in agreement with the theory

of aperiodic EDP and Equation 7 in the main text.

Figures S9-S10 show snapshots of cell and average intensity during experiments designed to measure migration velocity under aperiodic EDP. The position of the ensemble of particles is extracted by tracking the maximum intensity within the cell. To construct the curves of velocity shown in Figure 6 of the main text, two experiments were performed. In one experiment, particles were allowed to sediment at the bottom electrode; in the other, particles sedimented and started from the top electrode. Given the much higher velocity near the bottom electrode, only a volume covering 20 microns in height was imaged to increase the time resolution of the measurements. To measure the downward velocity, the cell was imaged from top to bottom electrodes. The last section provides details and additional plots with results for the model. The governing equations and the parameters used in the calculations are provided.

Contrasting pH and intensity maps for experiments at different voltages.

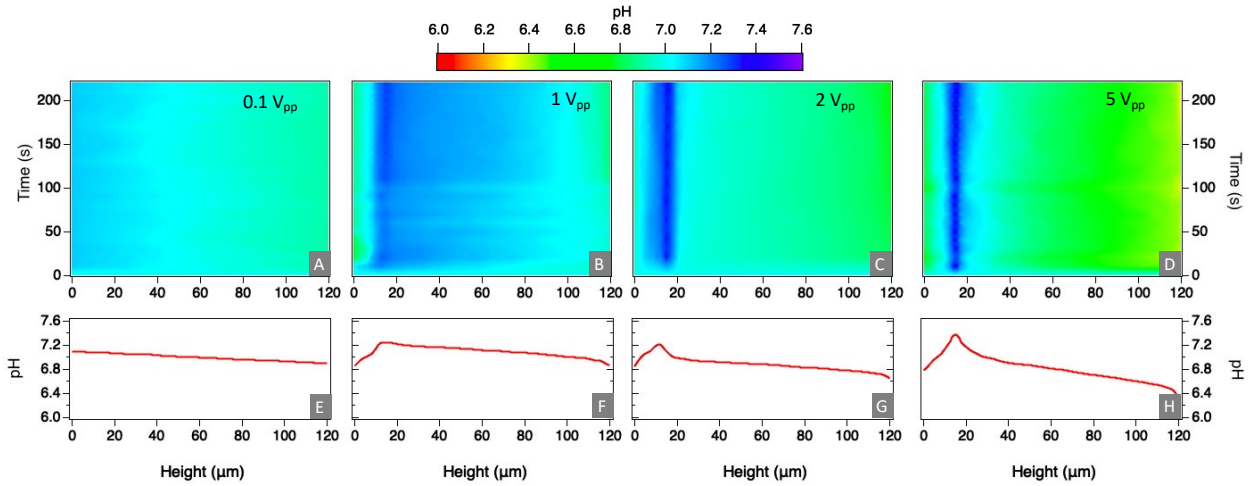

Figure S1: Comparison of pH profiles under different voltages. Panels (A-D) are 2D heat maps that show the established pH profiles during an experiment, while Panels (E-H) represent the pH profiles at the end of the experiment (220 s). The applied voltages were 0.1 (A, E), 1 (B, F), 2 (C, G) and 5 V_{pp} (D, H). The frequency was kept constant at 100 Hz. This data shows that higher voltages lead to more nonlinear pH profiles.

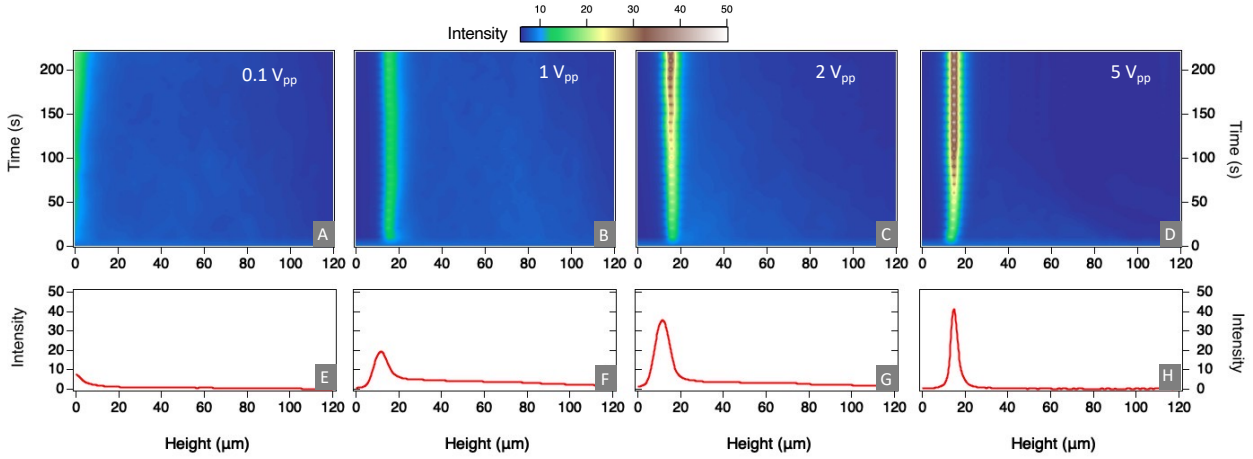

Figure S2: Comparison of electrokinetic response of charged particles (-65.5 ± 1.6) under different voltages. Panels (A-D) are 2D heat maps that show the established intensity profiles during an experiment, while Panels (E-H) represent the intensity profiles at the end of the experiment (220 s). The applied voltages were 0.1 (A, E), 1 (B, F), 2 (C, G) and 5 V_{pp} (D, H). The frequency was kept constant at 100 Hz. The rate of migration of particles towards the focusing position is strongly dependent on the applied voltage and the magnitude of the resultant pH gradients.

Contrasting pH and intensity maps for experiments at different frequencies.

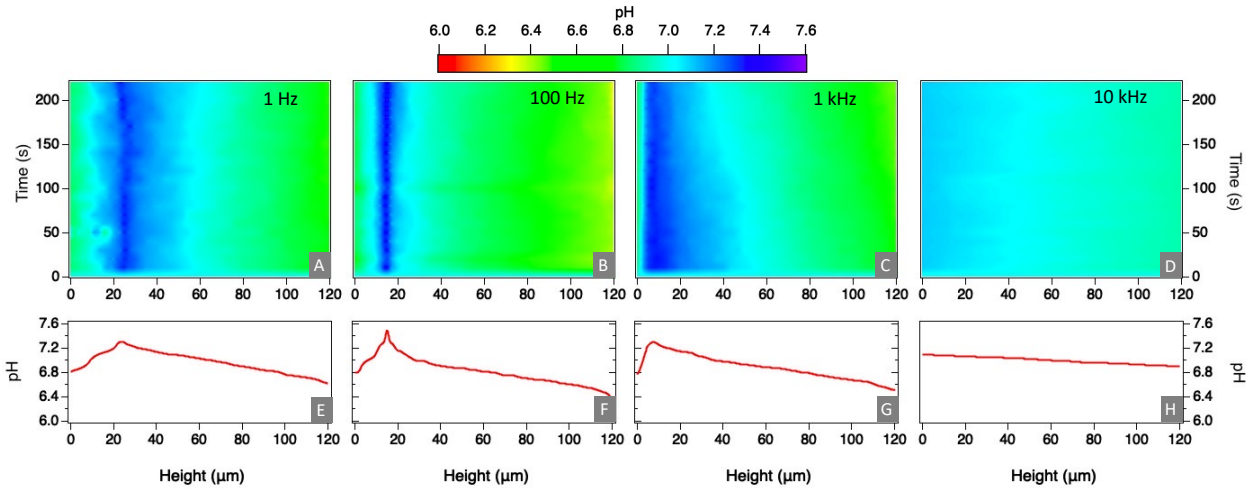

Figure S3: Comparison of pH profiles under different frequencies. Panels (A-D) are 2D heat maps that show the established pH profiles during an experiment, while Panels (E-H) represent the pH profiles at the end of the experiment (220 s). The applied voltages were 1 Hz (A, E), 100 Hz (B, F), 1 kHz (C, G) and 10 kHz (D, H). The voltage was kept constant at 5 V_{pp}. This data shows that frequency affects the shape and position of maxima in pH.

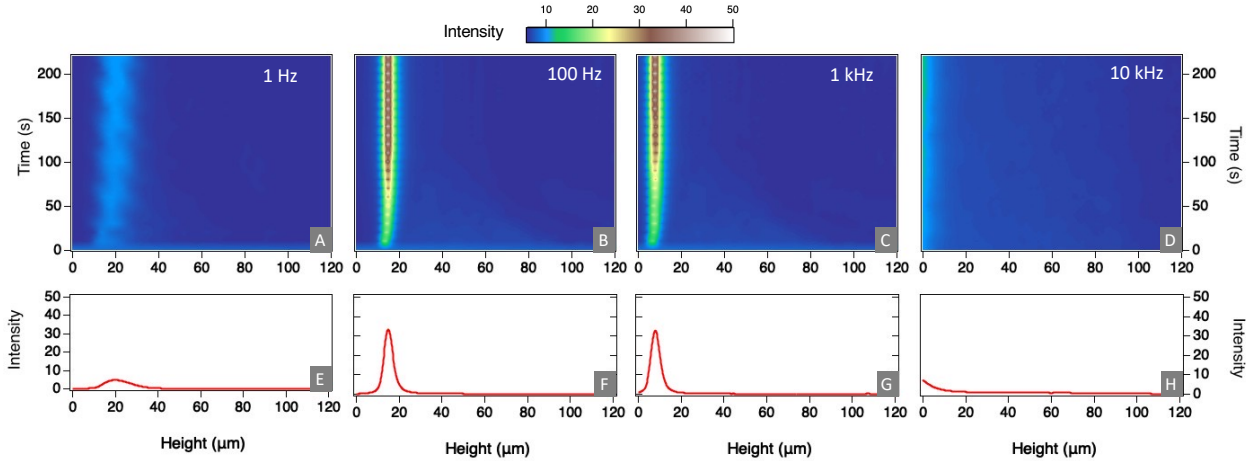

Figure S4: Comparison of electrokinetic response of charged particles (-65.5 ± 1.6) under different voltages. Panels (A-D) are 2D heat maps that show the established intensity profiles during an experiment, while Panels (E-H) represent the intensity profiles at the end of the experiment (220 s). The applied voltages were 1 Hz (A, E), 100 Hz (B, F), 1 kHz (C, G) and 10 kHz (D, H). The voltage was kept constant at 5 V_{pp}. This data shows that frequency affects the position of focusing and the rate of migration. Nonlinear pH gradients cease to form at frequencies above 1.7 kHz.

Contrasting pH and intensity maps for experiments at different initial pHs.

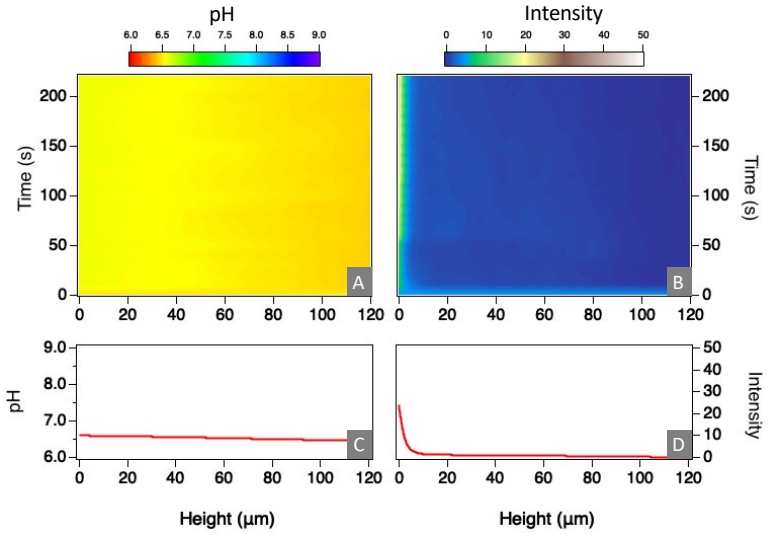

Figure S5: Juxtaposition of the pH map and the particle intensity map for experiments with initial $pH_0 \approx 6.5$. Panels A-B are 2D heat maps that condense the pH profiles and the fluorescence intensity from the particles, for all times in a single experiment. Panels (C-D) represent the pH and intensity profile for a single time (220 s). The applied signal was 5 V_{pp} and 100 Hz. Notice how steep gradients in pH are absent when the initial pH is sufficiently acidic. In this case, particles barely move, and the accumulation of particles at the bottom electrodes occurs due to gravity.

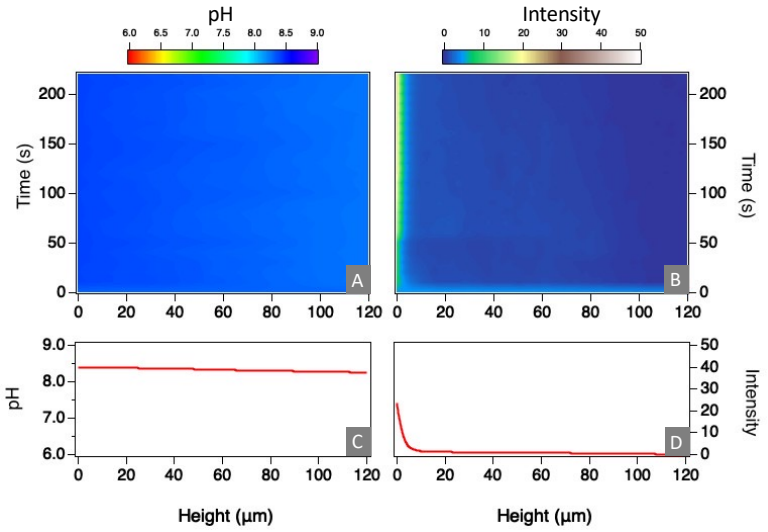

Figure S6: Juxtaposition of the pH map and the particle intensity map for experiments with initial $pH_0 \approx 8.4$. Panels A-B are 2D heat maps that condense the pH profiles and the fluorescence intensity from the particles, for all times in a single experiment. Panels (C-D) represent the pH and intensity profile for a single time (220 s). The applied signal was 5 V_{pp} and 100 Hz. Notice how steep gradients in pH are absent when the initial pH is sufficiently acidic. In this case, particles barely move and the accumulation of particles at the bottom electrodes occurs due to gravity.

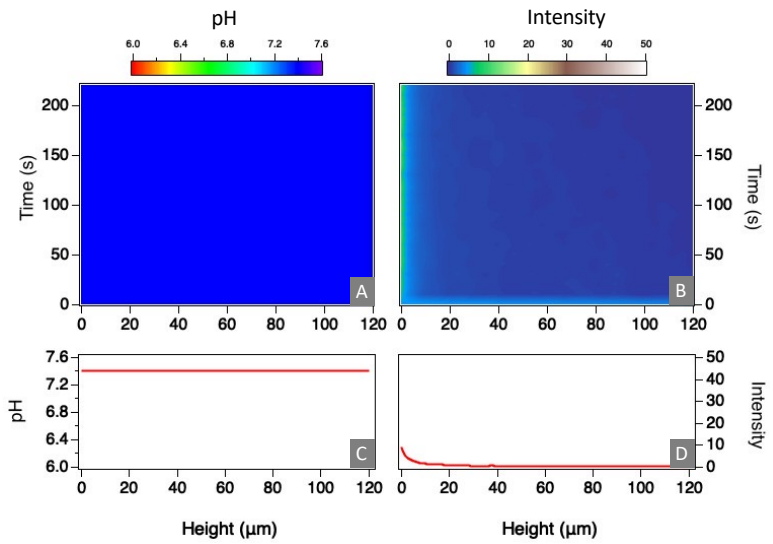

Figure S7: Juxtaposition of the pH map and the particle intensity map for experiments with PBS buffer and initial $pH_0 \approx 7.4$. Panels A-B are 2D heat maps that condense the pH profiles and the fluorescence intensity from the particles, for all times in a single experiment. Panels (C-D) represent the pH and intensity profile for a single time (220 s). The applied signal was 5 V_{pp} and 100 Hz. Notice how steep gradients in pH are absent in the presence of a pH buffer. In this case, particles barely move and the accumulation of particles at the bottom electrodes occurs due to gravity. This is evidence that pH gradients are necessary to observed migration and focusing of particles.

Contrasting pH and intensity maps for experiments at different concentration of supporting electrolyte.

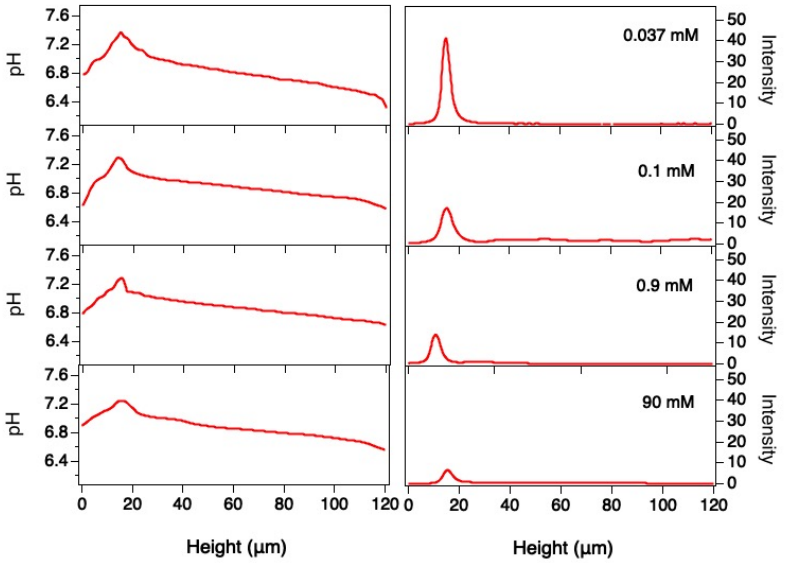

Figure S8: Response of particles at different concentrations of NaSCN. The left column shows the pH profiles at steady steady, while the column on the right shows the fluorescent intensity of particles after 220 s. The concentration of indifferent electrolyte affects the migration of particles. Although the pH profile remains fairly consistent, the intensity at the focusing position decreases with concentration of NaSCN. This observation is consistent with the prediction from Equation 7 in the main text. The applied signal was 5 V_{pp} and 100 Hz.

Measurements of velocity under aperiodic EDP: examples of images and analysis.

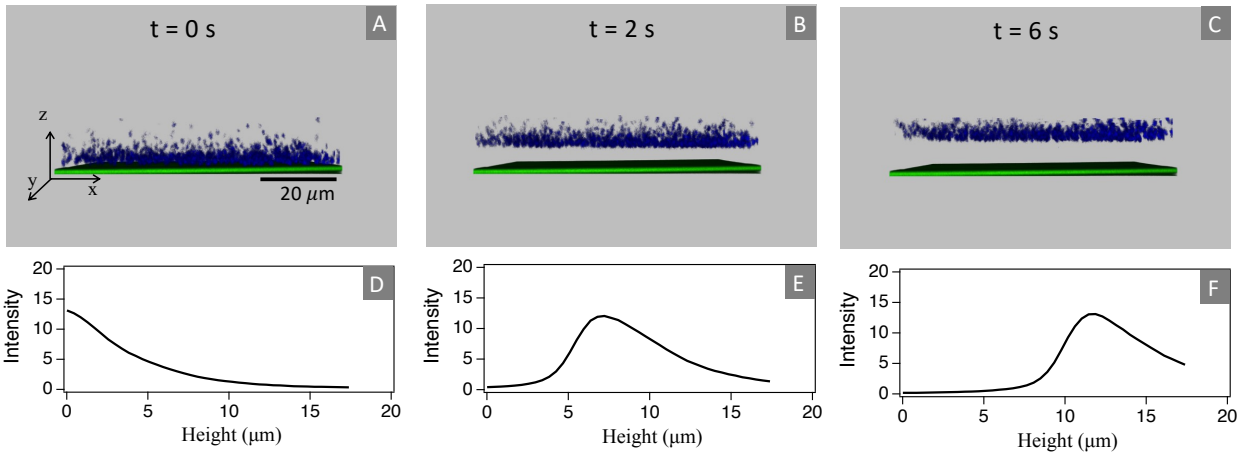

Figure S9: Velocity under aperiodic EDP can be extracted by tracking the emission intensity from the ensemble of particles. (A) To measure the upward velocity, particles are allowed to sediment on the bottom electrode for several hours with the field off. Once field is turned on, particles move towards the focusing point (B and C). The average position of the ensemble is estimated by the location of the peak in intensity (D-F). The frequency and voltage in this example are 100 Hz and 5 V_{pp}.

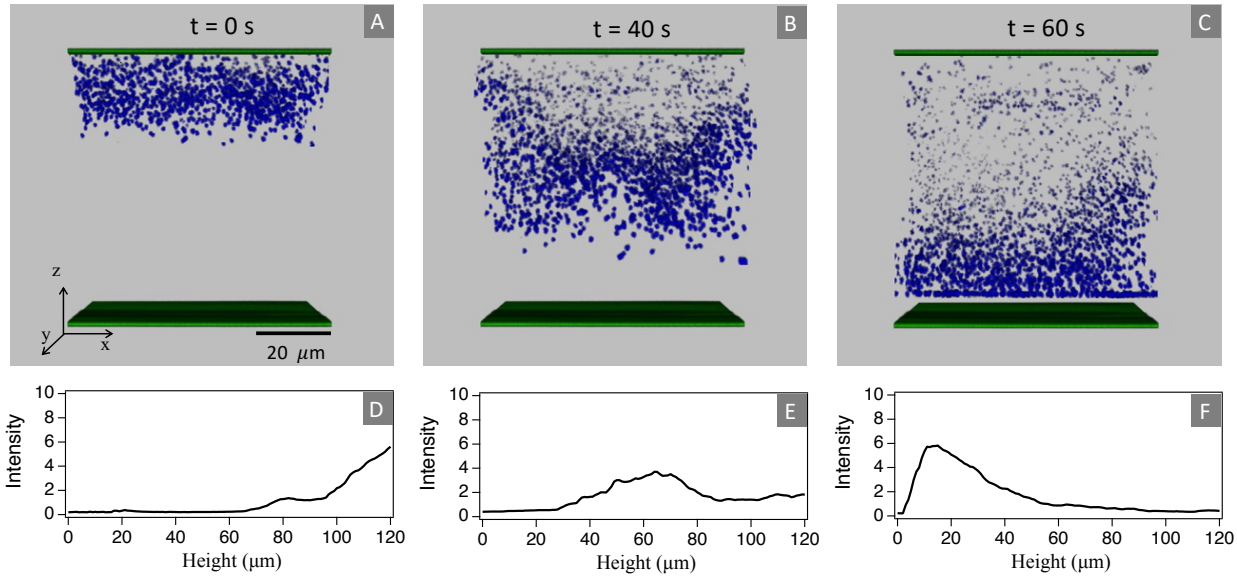

Figure S10: (A) To measure the downward velocity, particles are allowed to sediment on the top electrode for several hours with the field off. Once field is turned on, particles move towards the focusing point (B and C). The average position of the ensemble is estimated by the location of the peak in intensity (D-F). The frequency and voltage in this example are 100 Hz and 5 V_{pp}.

Analysis: calculation of pH profiles through a transport model.

A transport model that includes the conservation of charged species and the Nerst-Planck equations is solved to find the distribution of charged species within the electrochemical cell when an oscillating voltage is applied. Furthermore, given the oscillating nature of the field, we assume that transport of ions by migration is negligible. Therefore, under such conditions, the problem reduces to solving for mass transport. The governing equations are the following,

$$\frac{\partial C_j}{\partial t} + \nabla \cdot j_j = R_j, \tag{1}$$

$$j_j = -D_j \nabla C_j. \tag{2}$$

In these equations, C_j, j_j, and D_j represent the concentration (n_i in the main text), flux, and diffusivity of each species. R_j stands for the rate of generation of each species in the electrolyte or liquid domain. In our case, the ions are generated or consumed due to the equilibrium reaction of water, or dissociation of SNARF-1, within the liquid domain. The equations were solved for cases that included only H^+ and OH^+, and for cases that included SNARF-1 ions (and their dissociation reactions) as well. The equations are written following the notation for the variables as they appear in COMSOL.

The equations are solved with flux boundary conditions for each species,

$$-n \cdot j_j = \frac{-\nu_j i_{OC}}{nF}. \tag{3}$$

ν_j is the stoichiometry coefficient and i_{OC} is the local current density at the electrode surface; n stands for the number of electrons participating in the reaction, and F is the Faraday constant. The local electrode current density (i_{OC}) was calculated using the linearized Butler-Volmer relation:

$$i_{OC} = i_0 \frac{(\alpha_a + \alpha_c)\, F}{RT} \eta. \tag{4}$$

i_0, α_a and α_c represents the exchange current density, the anodic and cathodic transfer

coefficient, respectively. R and T are the universal gas constant and temperature. The constitutive equation for the exchange current density accounts for gradients of electroactive species,

$$i_0 = i_{0,ref} \prod_{j:\nu_j>0} \left(\frac{C_j}{C_{j,ref}}\right)^{(\alpha_c \nu_j/n)} \prod_{j:\nu_j<0} \left(\frac{C_j}{C_{j,ref}}\right)^{(-\alpha_a \nu_j/n)}, \tag{5}$$

$C_{j,ref}$ are the reference concentrations of each species. The overpotential (η) was determined by the following equation:

$$\eta = E_{ct} - E_{eq}, \tag{6}$$

$$E_{ct} = \phi_{s,exter} - \phi_l. \tag{7}$$

$\phi_{s,exter}$ and ϕ_l are the potentials applied externally and within the electrolyte potential, respectively. The equilibrium potential E_{eq} was determined through Nernst equation, while accounting for the concentration overpotential due to the pH gradient:

$$E_{eq} = E_{eq,ref} - \left(\frac{RT}{nF}\right) ln \prod_j \left(\frac{C_j}{C_{j,ref}}\right)^{(\nu_j)}, \tag{8}$$

$E_{eq,ref}$ is the reference equilibrium potential for the electrolysis of water at initial pH of 7. $E_{eq,ref}$ was calculated using a Pourbaix plot. The reactions at the electrodes (boundaries) were driven by oscillating voltages at one of the electrodes,

$$\phi_s = \phi_0 \sin(2\pi t f_r), \tag{9}$$

f_r stands for the frequency of the ac signal. The second electrode stayed grounded.

The models was solved using the Comsol electrochemsitry module (tertiary current distribution) with the Nernst-Planck interface. In this module, the constitutive equations stated above are readily available. The mesh was predefined as "extremely fine in the domain, with a fixed number of elements (1000) near the electrodes. The transient model was solved up to 20 s after the ac field is applied, with a time step equal to 0.1 s. The parameters used to

perform the calculations in COMSOL Multiphysics and the calculation of EDP velocity (using equations 7-8 of the main text) are listed in tables S1 and S2, respectively. Approximate values for the exchange current densities were obtained by measuring the current density through linear sweep voltammetry (LSV). The cathodic and anodic exchange current were extracted using a Tafel plot (Figure S11). The exchange current densities were obtained through the Tafel plot, as the intercepts at the x-axis. LSV was performed from -5 to +5 V, with a step size of 5 mV through the electrochemical device.

Table S1: Parameters used in Multiphysics simulation

Parameter	Symbol and Units	Value
Diffusivity, OH^-	D_{OH^-} (m^2/s)	5.00×10^{-9}
Diffusivity, H^+	D_{H^+} (m^2/s)	9.30×10^{-9}
Exchange Current Density, Anode	$i_{0,ref1}$ (A/m^2)	1.40×10^{-3}
Exchange Current Density, Cathode	$i_{0,ref1}$ (A/m^2)	4.00×10^{-3}
Reference Equilibrium Potential, Redox Reaction	E_{eq} (V)	8.20×10^{-1}
Reference Equilibrium Potential, Oxidizing Reaction	E_{eq} (V)	4.10×10^{-1}
Temperature	T (K)	2.98×10^{2}
Faraday Constant	F (sA/mol)	9.65×10^{5}
Reference Concentration, OH^-	$C_{OH^-,ref}$ (Mol/m^3)	1.60×10^{-4}
Reference Concentration, H^+	$C_{H^+,ref}$ (Mol/m^3)	6.31×10^{-5}
Anodic Transfer Coefficient	α_a	0.50
Cathodic Transfer Coefficient	α_c	0.50
Stoichiometric Coefficient, OH^-	ν_{OH^-}	1
Stoichiometric Coefficient, H^+	ν_{H^+}	-1
Number of Participating Electrons	n	1
Initial pH	pH_0	7.2

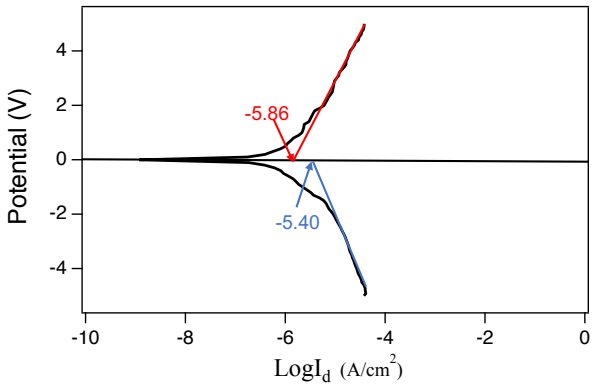

Figure S11: Tafel plot obtained through LSV . Both the positive and negative Tafel plots were linear fitted (red and blue line). The X-axis intercept, which is log (i_0,ref) was determined as -5.86 (positive LSV) and -5.40 (Negative LSV) respectively.

Table S2: Parameters used to perform EDP velocity calculations

Parameter	Symbol and Units	Value
Permittivity of Vacuum	$\varepsilon_0(\mathrm{C^2m^2/N})$	8.85×10^{-12}
Rel. Dielectric Constant, H_2O	ε_w	8.00×10^{2}
Elementary Charge	e (C)	1.60×10^{-19}
Avogadro's Number	N_A (1/mol)	6.02×10^{23}
Boltzmann constant	K_B ($\mathrm{m^2kg/s^2K}$)	1.38×10^{-23}
Temperature	T (K)	2.98×10^{2}
Thermal Energy	K_BT (J)	4.11×10^{-21}
Thermal Potential	K_BT/e (V)	2.57×10^{-2}
Viscosity	μ (Pa·s)	1.00×10^{-3}
Diffusivity, OH^-	D_{OH^-} ($\mathrm{m^2/s}$)	5.00×10^{-9}
Diffusivity, H^+	D_{H^+} ($\mathrm{m^2/s}$)	9.30×10^{-9}
M_-	s/kg	1.86×10^{11}
M_+	s/kg	-1.00×10^{11}
Zeta Potential	$\zeta e/K_BT$ (V)	-2.53
Bulk Concentration	$n_0^B(\mathrm{mol/m^3})$	0.10

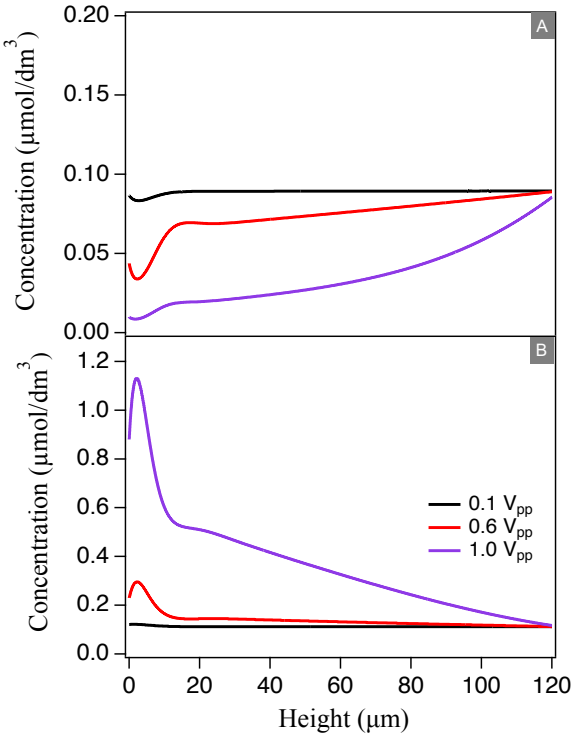

Figure S12: Concentration for (Panel A) H^+ and (Panel B) OH^- generated by solving the transport model at 100 Hz, and different oscillating voltages at the bottom electrode.

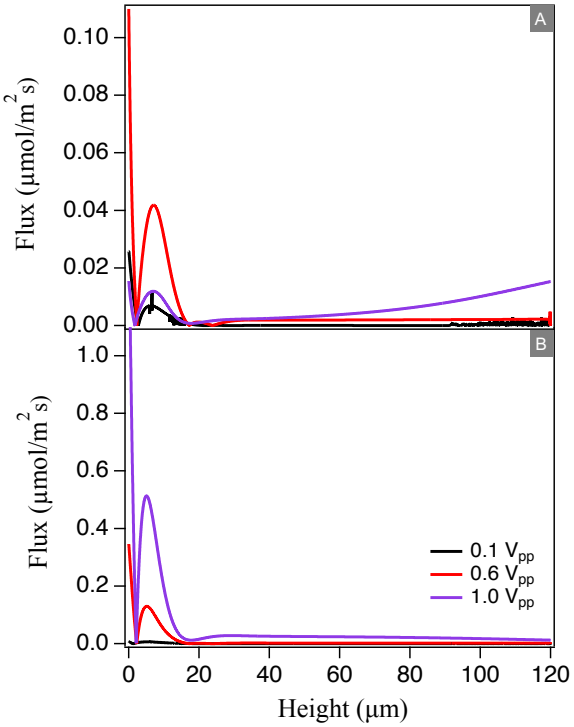

Figure S13: Ionic total flux magnitude for (Panel A) H^+ and (Panel B) OH^- generated by solving the transport model at 100 Hz, and different oscillating voltages at the bottom electrode.

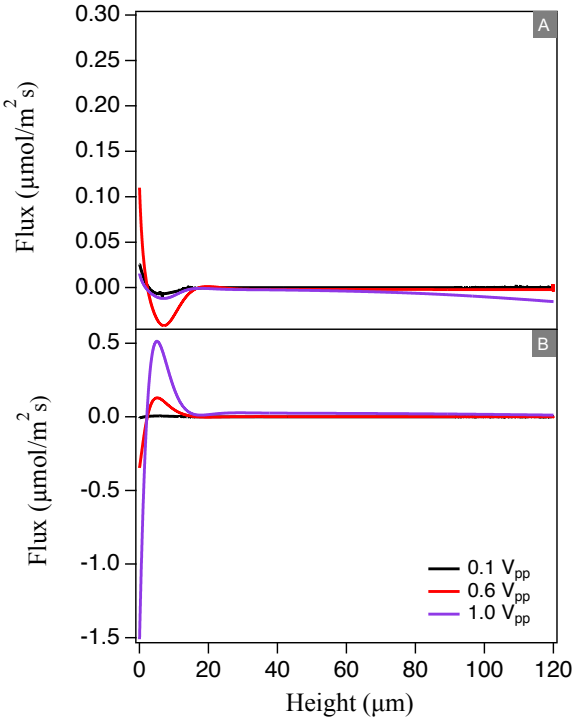

Figure S14: Ionic total flux for (Panel A) H^+ and (Panel B) OH^- generated by solving the transport model at 100 Hz, and different oscillating voltages at the bottom electrode.